Reduced HMGB1 expression contributed to lapatinib-induced cutaneous injury

Li Yu Jiang
Zhejiang University
Yan Zeng
Zhejiang University
Lei Lei Ai
Zhejiang University
Hao Yan
Zhejiang University
Xiao Chun Yang
Zhejiang University
Pei Hua Luo
Zhejiang University
Bo Yang
Zhejiang University
Zhifei Xu (xzfzjut@zju.edu.cn)
Zhejiang University
Qiao Jun He
Zhejiang University

Research Article

Keywords: Lapatini, cutaneous toxicity, apoptosis, DNA damage, HMGB1, saikosaponin A

Posted Date: March 21st, 2022

DOI: https://doi.org/10.21203/rs.3.rs-1461458/v1

Abstract

Lapatinib, a widely-used dual inhibitor of human epidermal growth factor receptor 1 (EGFR/ERBB1) and 2 (HER2/ERBB2), has been seriously limited due to cutaneous toxicity. However, the specific mechanism of lapatinib-induced cutaneous toxicity has not been clarified, leading to a lack of effective strategy to improve clinical safety. Here, we found that lapatinib could induce mitochondrial dysfunction, lead to DNA damage and finally cause apoptosis of keratinocytes. In addition, we found that lapatinib could induce aberrant immune response and promote the release of inflammatory factors *in vitro* and *in vivo*. Mechanistically, downregulated expression of DNA repair protein HMGB1 played a critical role in these toxic reaction processes. Overexpression of HMGB1 could inhibit keratinocyte apoptosis and inflammation reaction. Therefore, recovering the HMGB1 expression might be an effective remedy against lapatinib-induced cutaneous toxicity. Finally, we found that saikosaponin A could significantly rescue the reduced HMGB1 transcription, which could alleviate lapatinib-induced DNA damage, inhibit keratinocyte apoptosis and further prevent toxicity of lapatinib in mice. Collectively, our study might bring new hope to clinicians and tumor patients, and shed new light on the prevention of cutaneous adverse drug reactions induced by EGFR inhibitors.

Introduction

Lapatinib is an oral small-molecule dual tyrosine kinase inhibitor of human epidermal growth factor receptor 1 (EGFR/ERBB1) and 2 (HER2/ERBB2) (Moreira & Kaklamani, 2010). It has been indicated in combination with capecitabine for ERBB2-positive, previously-treated, advanced or metastatic breast cancer, which has been the most common malignancy in women worldwide (Medeiros & Allan, 2019). For breast cancer patients who have failed anthracycline-, taxane-, and trastuzumab-based therapy, lapatinib combined with capecitabine provides an effective therapeutic option (Moreira & Kaklamani, 2010). However, multiple clinical trials reported that cutaneous adverse effects occurred during lapatinib treatment, which has become increasingly prominent and serious, with an incidence of up to 54.9% (Sonnenblick, de Azambuja et al., 2016). What's worse, owing to the lacking of mechanism-based therapeutic regimen, severe cutaneous adverse effects may result in dose modifications or treatment interruption, eventually leading to tumor progression and the reduction of survival quality (Friedman, Lacouture et al., 2016). Hence, researches on the precise mechanism underlying lapatinib-induced cutaneous toxicity are urgently desirable.

The clinical manifestations of lapatinib-induced cutaneous toxicity mainly include rash, dermatitis acneiform, pruritus and generalized xerosis (Sonnenblick et al., 2016, Tischer, Huber et al., 2017). These toxic reactions are often accompanied by obvious epidermal damage, which manifested as inflammation, partial or severe epidermal scales or even exfoliation (Hoetzenecker, Nageli et al., 2016, Macdonald, Macdonald et al., 2015). The epidermal tissue of skin is mainly composed of keratinocytes, and studies have shown that keratinocytes are essential for maintaining the normal physiological function of the epidermal tissue (Simpson, Patel et al., 2011). As described in previous studies reported by our and other teams, small molecule kinase inhibitors (SMKIs) could induce cutaneous toxicity by

affecting keratinocyte fate, such as promoting cell death directly, regulating cell hyper-differentiation, migration and incomplete keratinization (Chen, Chen et al., 2017, Jin, Chen et al., 2021, Luo, Yan et al., 2020). More importantly, keratinocyte apoptosis has been determined to be involved in the pathological process of various skin diseases such as skin injury, erythema, dermatitis and alopecia (Fabbrocini, Panariello et al., 2015, Tang, Tu et al., 2018). It was reported that severe drug-induced cutaneous reactions like Stevens-Johnson syndrome (SJS) and toxic epidermal necrolysis (TEN) are characterized by keratinocyte apoptosis (Ergen & Hughey, 2017, Zhang, Zhu et al., 2020). Here, we observed a significantly reduction in keratinocytes at the epidermal layer in mice treated with lapatinib, and we firstly identified whether the high incidence of lapatinib-induced cutaneous toxicity is attributed to keratinocyte apoptosis in this study. In addition, inflammatory infiltration was found in the epidermis, which is in line with the clinical manifestation.

High mobility group box 1 (HMGB1) is a non-histone nucleoprotein, which is widely distributed and richly expressed in heart, liver, lungs, lymphoid tissue, brain and skin tissue (Mou, Liu et al., 2017). The function of HMGB1 mainly depends on subcellular localization (Kang, Chen et al., 2014). Numerous studies have uncovered that HMGB1 orchestrates the inflammatory and immune response as a damage associated molecular pattern molecule (DAMP) when it is released outside the cell (Kang, Livesey et al., 2011, Zhu, Messer et al., 2015). However, there is still lacking the attention focused on the nuclear HMGB1, that acts as a DNA chaperone, with the ability of binding to DNA and promoting DNA bending, and in turn plays an important role in regulating gene transcription, DNA damage repair, chromatin remodeling and stabilizing nucleosome structure (Kang et al., 2014). Furthermore, it has been reported that HMGB1 is highly expressed in keratinocytes and is closely associated with drug-induced skin disorders (Mou et al., 2017). Decreased epidermal content of HMGB1 has been identified in drug-induced SJS/TEN, raising the possibility that the analysis of HMGB1 in keratinocytes may represent a potential diagnostic marker of cell death/tissue damage in SJS/TEN (Carr, Wang et al., 2019). In addition, studies have provided evidence to support the notion that HMGB1 function to attenuate the expression of interleukin-24 (IL24) by chromatin remodeling, thereby protecting against dermatitis (Senda, Yanai et al., 2021). These findings above have underscored the unprecedented function of HMGB1 in skin disorders, however, the precise mechanism underlying HMGB1 mediating the drug-induced skin injury has yet to be clarified. Our RNA-sequencing (RNA-Seq) results revealed that HMGB1 is a co-changing gene in DNA damage and inflammatory response pathway, which prompts us to further investigate the significance of HMGB1 on lapatinib-induced cutaneous toxicity.

In this study, we found that lapatinib could promote mitochondrial dysfunction and subsequent DNA damage, which finally led to the apoptosis of keratinocytes and the occurrence of cutaneous toxicity. Meanwhile, we observed that the release of inflammatory factors was involved in this process *in vitro* and *in vivo*. Mechanistically, the transcription inhibition of HMGB1 played a critical role and overexpression of HMGB1 could inhibit DNA damage and keratinocyte apoptosis, indicating that HMGB1 could be a potential therapeutic target against lapatinib-induced cutaneous toxicity. Based on the findings, we identified saikosaponin A, a natural product from *Bupleurum chinensis* DC, could significantly alleviate lapatinib-induced DNA damage and inhibit keratinocyte apoptosis through recovering HMGB1

transcription, hence, providing potentially promising therapeutic strategies for the treatment of this toxicity.

Material And Methods

Animal experiments.

C57BL/6 female mice weighing 20-23g were purchased from Beijing Vital River Laboratory Animal Technology Co., Ltd. (Beijing, China). The mice were housed in barrier facilities with a 12-hour light/dark cycle. Before performing the experiments, one-week period allowed the mice to adapt to the laboratory environment, during which sufficient food and water were provided. Lapatinib and saikosaponin A were dissolved in 0.5% sodium carboxymethyl cellulose to obtain stock solution. The mice were treated with 950 mg/kg lapatinib or 20 mg/kg saikosaponin A or lapatinib plus saikosaponin A in experimental group through intragastric administration for 28 days. Correspondingly, the mice in control group were treated with the same volume of 0.5% sodium carboxymethyl cellulose (CMC-Na). The entire procedure was performed under an approved anesthetic protocol with pentobarbital sodium (45 mg/kg) to adequately sedate the mouse for the process.

Histopathological analysis.

Skin samples were obtained from the abdomen of mice were fixed in 10% phosphate-buffered formalin (pH = 7.4) (Sigma-Aldrich, F8775), embedded in paraffin and sectioned at 5 μm intervals. After dewaxing and rehydration, the sections were stained with hematoxylin and eosin (H&E) on glass slides (Beyotime, C0105) according to the instructions. For mast cell toluidine blue staining, 0.5% toluidine blue staining solution (1 g of toluidine blue (Sigma-Aldrich, 198161) in 200 mL 70% ethanol and filtered before use) was prepared. Paraffin embedded sections were mounted onto slides and dewaxed to water and subjected to 95% ethanol for 30 s, then the sections were incubated with toluidine blue staining solution at room temperature for 60 min. After that, the acid alcohol (0.5% HCl in 100 mL 95% ethanol) was used to rinse until sections were colorless. Finally, histopathological analysis was examined by microscopy.

TUNEL assay.

Apoptosis for formalin-fixed and paraffin-embedded skin sections was determined using a One Step TUNEL apoptosis assay kit (Beyotime, C1088) according to the manufacturer's instructions. Nuclei were stained with DAPI (Dojindo, D212) and the TUNEL signals were observed with fluorescence microscopy (Olympus, IX81-FV1000). Cell apoptosis was determined as the ratio of the number of TUNEL-positive nuclei to that of DAPI-positive nuclei.

Cell culture.

Human immortal keratinocyte line (HaCaT) was purchased from the Institute of Biochemistry and Cell Biology (Shanghai, China). Normal human epidermal keratinocytes (NHEK) from single donor (C-12003) were purchased from Promocell (Heidelberg, Germany). The cells were maintained in DMEM (Gibco, 10569010) supplemented with 10% fetal bovine serum (Gibco, 10099141) with 100 U/mL penicillin and 100 μg/mL streptomycin in a humid atmosphere of 5% CO_2 and 95% air at 37℃. After 3–5 passages, keratinocytes were used for subsequent experiments. HaCaT and NHEK cells used in this study were routinely tested to be negative for mycoplasma contamination.

Regents and antibodies.

Lapatinib (231277-92-2) was purchased from TargetMol (Boston, USA). For in-vitro assay, the concentration of the lapatinib stock solution was 8 mM prepared with dimethyl sulfoxide (DMSO; Sigma-Aldrich, D4540). Saikosaponin A (20736-09-8) was purchased from FEIYU Bio (Nantong, China), and 30 mM stock solution was prepared using DMSO in accordance with the manufacturer's recommendations. Z-VAD-FMK (187389-52-2) was obtained from Selleck Chemicals (Houston, USA). Antibodies against c-PARP (ET1608-10), c-CASP3 (ET1608-64) and HMGB1 (ET1601-2) were purchased from HuaBio (Hangzhou, China). Antibodies against phospho-histone H2A.X (G-H2A.X; #9718S), EGFR (#8504) and ERBB2 (34290) were purchased from Cell Signaling Technology Inc (Beverly, USA). Antibodies against ACTB (db7283) was purchased from diagbio (Hangzhou, China). Cytokeratin 5 (AF0194) was purchased from Affinity Biosciences Inc (Cincinnati, USA). Horseradish peroxidase (HRP)-labeled secondary antibody (GAR007) against primary antibodies was purchased from MultiSciences (Lianke) Biotech (Hangzhou, China).

Cell survival fraction assay.

Sulphorhodamine B (SRB; Sigma-Aldrich, S1402) assay of cellular protein biomass was used to assess cell viability as previously described (Xu, Jin et al., 2018). In brief, cells (5×10^3/well) were plated and treated in 96-well plates and left for 24-hour growth in 5% carbon dioxide incubator at 37°C. After 24-hour drug treatment, cells were fixed with 10% (wt/vol) trichloroacetic acid for over 2 h at 4℃ and stained with SRB (dissolved in 1% acetic acid aqueous solution) for 30 min. Multiskan Spectrum (Thermo Electron Corporation, Marietta, USA) was used for absorbance measurement at 510 nm. The inhibition rate of cell proliferation was calculated for each well as the follow: (the absorbance of control cells - the absorbance of treated cells)/the absorbance of control cells) × 100%.

Western blot analysis.

After treatment, cells and skin tissues were harvested by resuspended in lysis buffer (compose of 50 mM Tris-HCl, 150 mM NaCl, 2 mM EDTA, 2 mM EGTA, 25 mM NaF, 25 mM B-Sodium Glycerophosphate, 0.3% NP-40, 0.3% Triton X-100, 0.3% Leupeptin, 0.1% PMSF and 0.1% NaVO3). Protein samples (10-20 μg per

sample) with loading buffer were boiled for 20 min and separated on 12% SDS-PAGE gels, and then transferred to PVDF membrane (Millipore Corporation, USA) in Tris-Glycine transfer buffer at 330 mA for 1 h. Primary antibodies were then added and incubated on a shaking table at 4℃ overnight followed by the incubation with secondary antibodies for another 2 h at room temperature. Finally, ECL-Plus Kit (PerkinElmer, MA, USA) was used to detect the bands and visualized on autoradiography film.

Apoptosis assay.

2×10^4 per well cells were seeded in 6-well plates and left for 24-hour growth in 5% CO2 incubator at 37°C. The cells were then exposed to the drug for indicated times and concentrations. At the end of the incubation period, the culture medium was removed and the cells were washed twice with cold phosphate-buffered saline (PBS; Gibco, 10010023) and harvested through trypsinization. FACS Calibur cytometer (BD, San Jose, USA) was used to analyze the apoptosis rate using a FITC Annexin V Apoptosis Detection Kit I (MultiSciences (Lianke) Biotech, AP101) according to the manufacturer's instructions.

Mitochondrial membrane potential detection.

Cells were treated and harvested as mentioned above, and then resuspended in 1mL PBS and moved to 1.5 mL centrifuge tube. 10 μg/mL JC-1 (Sigma-Aldrich, T4069) was added and the cells were incubated for 30 min at 37°C without light. After the incubation period, the cells were washed twice with PBS to remove the unbinding JC-1 and then resuspended in 500 μL PBS. FACS Calibur cytometer (BD, San Jose, USA) was used to analyze the change of mitochondrial membrane potential.

ROS measurement.

ROS was analyzed by using ROS detection kit (Beyotime, Shanghai, China) in accordance with its instruction. Briefly, cells were treated and harvested as mentioned above and resuspend in DCFH-DA working solution and incubated for 20 min at 37°C without light. After the incubation period, the cells were washed three times with FBS-free DMEM medium to remove the free DCFH-DA and then resuspended in 500 μL PBS. FACS Calibur cytometer (BD, San Jose, USA) was used for further analyzing and the signals were observed with fluorescence microscopy.

ELISA (enzyme linked immunosorbent assay).

Supernatants from C57BL/6 mice were used to determine the secretion of TNF-A by mouse precoated TNFA ELISA kit (DAKEWE, 1217202), and supernatants from cells were used to detect the secretion of TNFA or IL6 using human precoated TNFA ELISA kit (DAKEWE, 1117202) or human precoated IL6 ELISA kit (DAKEWE, 1110602) according to the manufacturer's protocol. Briefly, culture medium or whole blood sample was centrifuged at 1000 × g for 20 min to collect the supernatant. Supernatant samples or serial

dilutions of standard recombinant TNFA or IL6 were added at 50 μL/well in 96-well ELISA plate. After that, 100 μL of HRP-labeled detection antibody was added. Subsequently, the liquid in each well was discarded, and the plate was washed five times with washing buffer. Then, chromogenic solution and stop solution was added to each well successively (the interval is about 15 min), and the absorbance was read at a wavelength of 450 nm within 15 min. The absorbance values were converted to corresponding values in pg/mL based on the linear regression transformation of the standard curve.

Plasmid construction and infection.

HA-HMGB1 was generated by restriction digestion of the plasmids with EcoR1 plus NOT1, followed by ligations. Cells were transfected with plasmids using the Lipofectamine 2000 transfection reagent (Invitrogen, 11668-019) according to the manufacturer's instructions.

siRNA oligonucleotides transfection.

Cells were seeded into 6-well plates at 1.5×10^4 cells per well and grown to 50-60% confluence. Transfection was performed using jetPRIME (Polyplus-transfection, 114-15) according to the manufacturer's protocol. siRNA oligonucleotides were transfected at a final concentration of 12 nM. Cell culture solution was changed to fresh DMEM medium for further study. The following oligonucleotides were obtained from GenePharma (Shanghai, China) as siRNAs targeting the indicated genes:

Negative Control: 5'-UUCUCCGAACGUGUCACGUTT-3';

ERBB2 siRNA#1: 5'-GUGCCAAUAUCCAGGAGUUTT-3';

EGFR siRNA#1: 5'-CAAAGUGUGUAACGGAAUATT-3';

EGFR siRNA#2: 5'-GCAAAGUGUGUAACGGAAUAGGUAU-3';

HMGB1 siRNA#1: 5'-CCGTTATGAAAGAGAAATGAA-3'.

Quantitative real-time PCR (RT-qPCR).

The procedures were referred to the previous study (Luo, Yan et al., 2021). After treatment, cells were harvested with the Trizol reagent (Invitrogen, 15596-026). Equal amounts of RNA were reverse transcribed into complementary DNA with the cDNA reverse transcription kit (Transgene, AT311). RT-qPCR was performed on a 7500 Fast System (Applied Biosystems, Singapore) using the iTaq Universal SYBR Green Supermix (Bio-Rad, 172-5124), and variable ddH2O to generate a volume of 20 μL. The samples underwent two-step amplification with an initial step at 95°C (3 min), followed by 95°C (3 s) and 60°C (31 s) for 39 cycles. The melting curve was analyzed. Fold changes in the expression of each gene were calculated by the comparative threshold cycle (Ct) method using the formula 2-(ΔΔCt). Three

independent biological samples were quantified in technical duplicates and expression values were normalized to housekeeper gene.

The primer sequences were as follows:

GAPDH-Forward: 5’-TGATGACATCAAGAAGGTGGTGAAG-3’;

GAPDH-Reverse : 5’-TCCTTGGAGGCCATGTGGGCCAT-3’;

HMGB1-Forward: 5’-GATATGGCAAAAGCGGACAAG-3’;

HMGB1-Reverse: 5’-GGCGATACTCAGAGCAGAAG-3’;

TNFA-Forward: 5’-CTCACCCACACCATCAGC-3’;

TNFA-Reverse: 5’-GAAGACCCCTCCCAGATAGA-3’;

IL6-Forward: 5’-AAAAGTCCTGATCCAGTTCCTG-3’;

IL6-Reverse: 5’-TGAGTTGTCATGTCCTGCAG-3’;

CCL2-Forward: 5’-CCAATAGGAAGATCTCAGTGCAG-3’;

CCL2-Reverse: 5’-AATCCTGAACCCACTTCTGC-3’;

IL18-Forward: 5’-CATTGACCAAGGAAATCGGC-3’;

IL18-Reverse: 5’-CACAGAGATAGTTACAGCCATACC-3’;

Tnfa-Forward: 5’-GGTGCCTATGTCTCAGCCTCTT-3’;

Tnfa-Reverse: 5’-GCCATAGAACTGATGAGAGGGAG-3’;

Il6-Forward: 5’-TACCACTTCACAAGTCGGAGGC-3’;

Il6-Reverse: 5’-CTGCAAGTGCATCATCGTTGTTC-3’.

RNA-Seq analysis.

Cells were treated with or without lapatinib for 24 h and total RNA was isolated using Trizol reagent according to the manufacturer’s protocol. After purification, the mRNA was reverse transcribed to create 1 μg of final cDNA for the construction of sequencing libraries using Illumina TruSeq RNA Sample Prep Kit (FC-122-1001). The average insert size for the cDNA library was 300 ± 50 bp. The cDNA was then sequenced using a HiSeq 4000 system (Illumina) and a 150-bp paired-end run according to the manufacturer's instructions. Differential expression analysis was performed based on adjusted p-values,

GO enrichment and KEGG analysis of the differentially expressed mRNAs were also conducted. The RNA-Seq data were deposited in the NCBI's Gene Expression Omnibus database (GSE195713).

Immunofluorescence assay.

For *in-vitro* assay, cells were seeded on round cover slips in a 24-well plate one night in advance and treated with the drug as indicated time and concentration. After discarding culture medium, cells were fixed with fresh 4% paraformaldehyde (Sigma-Aldrich, P6148) in PBS for 20 min at room temperature. Next, cells were permeabilized with 0.1% Triton X-100 (Sigma-Aldrich, 9036-19-5) in PBS for 10 min at 4°C and blocked with 1% bovine serum albumin (BSA; Sigma-Aldrich, B2064) in PBS for 30 min at room temperature. For *in-vivo* assay, skin tissues were collected and fixed with fresh 4% paraformaldehyde overnight. Then the tissues were dehydrated with 30% sucrose (Sinopharm Chemical Reagent, 10,021,418) and embedded with Optimal Cutting Temperature (Sakura Finetek, 4583) to make frozen sections (8 μm). The sections were washed with PBS for 3 times and blocked with 1% BSA in PBS with 0.1% Tween-20 (Aladdin, T104863) for 30 min. Cells or sections were incubated with primary antibodies G-H2AX (diluted at 1: 200) or cytokeratin 5 (diluted at 1: 200) at 4°C overnight. After washed with PBS, the cells were incubated with Alexa Fluor 488- or Alexa Fluor 568-conjugated secondary antibodies (Thermo Fisher Scientific, A21202, A10042, 1:200) for 2 h, stained with DAPI for 5 min and mounted for fluorescence microscopy.

Comet assay.

The comet assay was performed as described previously. Firstly, single cell suspension was prepared at a density of about 2×10^4 cells/mL in PBS. Next, preheated 0.5% normal-gelling-temperature agarose were placed onto microscope slide, after ensuring that it has completely solidified, then 85 μL 0.5% low-gelling-temperature agarose with 10 μL single cell suspension and 0.5% low-gelling-temperature agarose were spread successively (placed for over 10 min in turn). The slides were dipped into alkaline solution (1% Triton X-100, 10% DMSO and 89% lysis buffer containing 10 mM Tris, 2.5 M NaCl and 100 mM Na_2EDTA with pH = 10) for 1 h at 4°C to lyse samples. The slides were placed in a horizontal electrophoresis chamber filled with cold alkaline solution (pH=12.3) for 20 min to unwind DNA and electrophoresis was conducted for 20 min at 300 mA (about 0.6 V/cm). Subsequently, the samples were taken out and neutralized with Tris-HCl (pH = 7.5) for 15 min and then dehydrated in 70% ethanol. The samples were then stained with DAPI in dark place for 6 min and captured images by fluorescence microscope. Using Comet Assay Software Project (CASP), the percentage of DNA in tail was scored per sample.

Statistical analysis.

Statistical analysis was performed using GraphPad Prism 9 software. All data were expressed as the mean value ± standard deviation (SD). When comparing two groups, Student's *t* test (unpaired, two-tailed)

was performed. Dunnett's multiple comparisons test was used to assess the significance of differences among treatment groups with a single control mean, and a Sidak test was used to assess the significance of differences among various pairs of groups. All experiments were repeated three times and *P* values were indicated in the figure legends.

Results

Lapatinib causes cutaneous toxicity and keratinocyte death.

Common and severe cutaneous toxicity has been a primary issue related to the clinical application of lapatinib in anticancer treatment. To mimic the occurrence of cutaneous toxicity and gain clearer insights into the specific mechanism, we first established an animal model of lapatinib-induced cutaneous toxicity by treating C57BL/6 mice with 950 mg/kg lapatinib daily for 28 days, which is 5–fold of clinical dose. It was found that the generalized xerosis and scales occurred in the skin tissue of mice treated with lapatinib (Fig. 1A). Referring to the clinical manifestation criteria, we divided the severity of scales into 4 grades: none, mild, moderate and severe, which were scored as 0, 1, 2 and 3, respectively. As shown in Fig. 1B, the score of scales in lapatinib-treated group was significantly higher than the control. Meanwhile, H&E staining results revealed that lapatinib could cause severe damage in mice skin tissue, mainly manifested as significant thickening of epidermal layer, intracellular edema and nuclear pyknosis of keratinocytes (Fig. 1C, D). To further validate the effect of lapatinib on keratinocytes, the main components of epidermis, we examined the expression of cytokeratin 5, a marker of keratinocytes, which is involved in maintaining the structural integrity of keratinocytes in the epidermis of skin (Atkinson, McGilligan et al., 2011, Ramirez, Bravo et al., 1994). Here, we found that the expression of cytokeratin 5 was almost invisible in the skin of mice treated with lapatinib, suggesting that lapatinib decreased the number of keratinocytes in mouse skin (Fig. 1E). Given that cutaneous toxicity, including rash, is often accompanied by inflammation, we next investigated TNFA level, which participates in normal immune response and is increased in many pathological conditions (Balkwill, 2006). When exposed to lapatinib, the concentration of TNFA in serum and the relative expression levels of *TNFA* and *Il6* in skin were all remarkably increased compared with the control group (Fig. 1F-H). Toluidine blue staining assay demonstrated the increase of hyperchromatic mast cells in the epidermis of the lapatinib-treated group compared to the control, suggesting that inflammation was involved in lapatinib-induced cutaneous toxicity (Fig. 1I). Taken together, we conclude that lapatinib indeed causes high-incidence and severe cutaneous toxicity *in vivo*.

Considering that lapatinib reduced the number of keratinocytes in lapatinib-induced cutaneous toxicity, we then focused on keratinocytes to clarify the toxic mechanism. We treated human immortalized keratinocytes HaCaT and normal human epidermal keratinocytes NHEK with lapatinib followed by SRB assay. Lapatinib was observed to decrease the survival fraction of both HaCaT and NHEK cell lines in a dose-dependent manner. Meanwhile, cell morphology of the lapatinib-treated cells demonstrated obvious shrinkage compared with that of the control group, suggesting that lapatinib might lead to keratinocyte apoptosis (Fig. 1J, K).

Lapatinib induces keratinocyte apoptosis in vitro and in vivo.

To further verify whether keratinocyte apoptosis contributes to lapatinib-induced cutaneous toxicity, we detected the protein levels of apoptosis markers, cleaved PARP (c-PARP) and cleaved caspase 3 (c-CASP3) under lapatinib treatment. The results showed that lapatinib significantly increased the protein levels of c-PARP and c-CASP3 in a dose- and time-dependent manner (Fig. 2A-D, Fig S1A, B), and this effect could be reversed by the pan-caspase inhibitor Z-VAD-FMK (Fig. 2E, F). Moreover, Z-VAD-FMK could rescue the cell death caused by lapatinib, which further proved that lapatinib could promote caspase-dependent apoptosis (Fig S1C). We next performed flow cytometry with PI/Annexin V double staining to detect the apoptosis rate under lapatinib treatment. Lapatinib significantly promoted the apoptosis of keratinocytes (Fig. 2G-J). According with the results of western blot, Z-VAD-FMK could partially reverse the apoptotic outcome induced by lapatinib (Fig S1D, E). Based on these *in-vitro* findings, we sought to explore whether keratinocyte apoptosis occurred *in vivo* by performing TUNEL assay. As illustrated in Fig. 2K, L, the number of TUNEL-positive (green fluorescence) keratinocytes was significantly increased in the epidermis of mice treated with lapatinib, indicating that lapatinib could induce DNA breakage and keratinocyte apoptosis *in vivo*. Taken together, these results suggest that lapatinib may induce cutaneous toxicity by activating caspase-dependent apoptosis.

RNA-Seq analysis reveals that lapatinib-induced keratinocyte apoptosis is related to mitochondrial dysfunction and DNA damage.

According to the results above, we then attempted to profile potential factors that might drive cutaneous toxicity of lapatinib by conducting RNA-Seq analysis. Following 24-hour treatment of lapatinib, transcriptome analysis identified that 2224 and 2019 genes were upregulated and downregulated, respectively (Fig. 3A). A subsequent comparison of the gene expression differences between the lapatinib-treated group and the control combined with Gene Ontology (GO) analysis revealed that these differentially expressed genes showed high enrichment in GO terms such as mitochondrion organization, DNA damage and repair (Fig. 3B), which was further confirmed by gene set enrichment analysis (GSEA) (Fig. 3C-E). Kyoto Encyclopedia of Genes and Genomes (KEGG) signaling pathway analysis and GSEA also reported that genes involved in DNA repair and apoptosis pathway were enriched in the downregulated and upregulated group, respectively (Fig S3A-D). Specifically, we observed decreased expression levels of DNA repair factors (*RRAD*, *BARD1* and *LIG1*, *etc.*) and increased expression levels of DNA damage factors (*ERCC5* and *BCL6*, *etc.*) in lapatinib-treated group (Fig. 3F, Fig S3E). These data indicate that lapatinib might promote the apoptosis of keratinocytes by inducing mitochondrial dysfunction and further DNA damage.

Inspired by the findings in Fig 3, we tended to further determine the significance of mitochondrial dysfunction in the keratinocyte apoptosis induced by lapatinib. Given that mitochondrial membrane potential loss is a significant sign of mitochondrial dysfunction (Ly, Grubb et al., 2003), here we applied flow cytometry combined with JC-1 staining to analyze the changes of mitochondrial membrane potential after 24 h lapatinib treatment. We found that lapatinib significantly increase the ratio of green to red fluorescence signals in keratinocytes, namely a significant decrease in mitochondrial membrane potential. Moreover, with the increase of lapatinib concentration, the proportion of keratinocytes with mitochondrial membrane potential loss continued to increase, indicating that lapatinib could cause mitochondrial dysfunction (Fig. 4A, B).

In addition, our experiments have demonstrated that lapatinib-induced keratinocyte apoptosis was accompanied by the transcriptional change of genes related to DNA damage and repair pathway. We then conducted the alkaline single cell gel electrophoresis (Comet) assay to investigate the occurrence of DNA damage. The degree of DNA damage showed a dose- and time-dependent increase with lapatinib stimulation through quantitative analysis of the length and intensity of the comet tail after electrophoresis (Fig. 4C, D and Fig S3A, B). As phosphorylation of H2A.X protein (G-H2A.X) has been recognized as a marker of DNA damage (Kuo & Yang, 2008), we then detected the protein level of G-H2A.X when keratinocytes were treated with lapatinib. The results showed that lapatinib significantly upregulated the protein level of G-H2A.X (Fig. 4E-H). Immunofluorescence assay showed that the accumulation of G-H2A.X puncta was increased in keratinocytes treated with lapatinib (Fig. 4I). These results suggested that lapatinib may induce DNA damage, consequently leading to the apoptosis of keratinocytes.

It has been reported that abnormal accumulation of ROS from mitochondrial metabolism is closely related to mitochondrial dysfunction, which may result in DNA damage (Circu & Aw, 2010, Nadanaciva & Will, 2009). We thus turned to identify whether abnormal ROS accumulation contributed to the keratinocyte apoptosis caused by lapatinib. The results of flow cytometry combined with DCFH-DA staining showed that ROS remarkably accumulated in a dose-dependent manner in response to lapatinib, which suggested that lapatinib-induced keratinocyte apoptosis might be related to abnormal ROS accumulation (Fig. 4J, K). Altogether, these results support that mitochondrial dysfunction, excessive ROS accumulation and DNA damage are involved in lapatinib-induced keratinocyte apoptosis.

The aberrant immune response is involved in lapatinib-induced cutaneous toxicity.

We have previously observed that lapatinib significantly increased the level of pro-inflammatory factors in skin and in serum (Fig. 1F-H). To further clarify the potential contribution of inflammation to lapatinib-induced cutaneous toxicity, we analyzed the changes in immune-related gene expression by RNA-Seq analysis. As listed in the heatmap, the expression of proinflammatory factors was upregulated, and in turn, the expression of anti-inflammatory factors was downregulated, implying the occurrence of

inflammation in keratinocytes in response to lapatinib (Fig. 5A). Next, we assessed the expression of inflammatory factors in keratinocytes under different periods of lapatinib treatment. Compared with the control group, the relative expression levels of *TNFA*, *IL6*, *CCL2* and *IL18* in HaCaT cells treated with lapatinib increased in a time-dependent manner, and sharply at 36 h, among which *CCL2* expression reached approximately four times of the normal level at 24 h (Fig. 5B). Similar results were observed in NHEK cells, and the obvious increases of *IL6* and *IL18* occurred earlier (Fig. 5C). Furthermore, we found that the concentration of IL6 in the supernatant of HaCaT cells exposed to 4 μM lapatinib for 48 h was significantly higher than that of the control group, while the concentration of TNFA showed no statistical difference after lapatinib treatment, indicating that IL6 rather than TNFA, might be the key factor to trigger the inflammatory reaction in keratinocytes under lapatinib stimulation (Fig. 5D). According to the time course of apoptosis and inflammation showed in Fig 2 and 5, we supposed that apoptosis was prior to the inflammation, and even further promoted the initiation of the latter. Several studies have reported that apoptosis is implicated in a wide range of patho-physiological stages, including autoimmune, bacterial, and viral disease. The critical role of apoptosis in eliminating harmful or injured cells from tissues suggests its participation in inflammatory processes (Onishi, Tanimoto et al., 1997, Van Opdenbosch & Lamkanfi, 2019). However, the expression of inflammatory factors displayed no detectable change when apoptosis was inhibited, which is inconsistent with our hypothesis and indicated that inflammation was not the downstream of apoptosis in the cutaneous toxicity induced by lapatinib (Fig S4). Together, these results suggest that aberrant inflammation is involved in the development of lapatinib-induced cutaneous toxicity.

Downregulation of HMGB1 expression mediates lapatinib-induced cutaneous toxicity.

Based on the above findings, it is reasonable to conclude that lapatinib could induce cutaneous toxicity by evoking DNA damage and apoptosis in keratinocytes. However, the key factor that mediates the detrimental effect remains unknown. It was known that some of skin side effects of SMKIs are correlate with on-target impact (Liu & Kurzrock, 2014), thus we first evaluated the relationship between the inhibition on the targets (*ERBB2* and *EGFR*) of lapatinib and keratinocyte apoptosis. No significant difference in c-PARP and c-CASP3 protein levels and survival fraction of keratinocytes was observed after knockdown/overexpression of *ERBB2* or *EGFR* (Fig S5). Thereafter, we set out to seek for the alternative target that possibly drove lapatinib-induced keratinocyte apoptosis. Our results showed that DNA damage, apoptosis and immune response in keratinocytes were involved in the cutaneous toxicity of lapatinib, which promoted us to identify the key regulators that could regulate these toxic processes through comparing the transcriptome of keratinocytes using RNA-Seq analysis. We found that upon lapatinib treatment, 155, 134 and 9 genes associated with cellular response to DNA damage, DNA repair and positive regulation of innate immune response differentially expressed, respectively. Interestingly, only one gene, *HMGB1*, overlapping among the set of misregulated genes was observed (Fig. 6A). In addition to the well-known function as an inflammatory cytokine after release,

intranuclear HMGB1 is of significance in regulating gene transcription, DNA damage repair, chromatin remodeling and stabilizing nucleosome structure (Kang et al., 2014). Abundant evidence supports that nuclear HMGB1 is essential for maintaining skin homeostasis (Senda et al., 2021). Thus, we envisaged that decreased HMGB1 expression might be the key event in lapatinib-induced cutaneous toxicity. Consistent with our hypothesis, *HMGB1* mRNA levels were reduced in a dose- and time-dependent manner under lapatinib treatment (Fig. 6B-E). The downregulation of HMGB1 protein level was also confirmed by western blot (Fig. 6F-I). Further *in-vivo* validation by western blot showed that, as expected, the expression of HMGB1 was significantly downregulated in the skin tissue of lapatinib-treated mice (Fig. 6J, K). These results suggest that the downregulation of HMGB1 expression might be involved in lapatinib-induced cutaneous toxicity.

To further corroborate that HMGB1 expression could modulate lapatinib-induced keratinocyte apoptosis and cutaneous toxicity, we applied siRNA to silence the expression of *HMGB1* to mimic the effects of lapatinib. As shown in Fig. 6L-N, knockdown of *HMGB1* increased the protein levels of DNA damage marker G-H2A.X, apoptosis-related protein c-PARP, and mRNA levels of inflammatory factors such as *IL6*, *CCL2* and *IL18*. In turn, overexpression of *HMGB1* significantly reduced the upregulation of G-H2A.X and c-PARP protein levels induced by lapatinib (Fig. 6O, P). Meanwhile, we observed a significant decrease in the inflammatory factor expression (Fig. 6Q). These findings implied that *HMGB1* overexpression could inhibit lapatinib-induced DNA damage, keratinocyte apoptosis and alleviate inflammation, while *HMGB1* overexpression showed no apparent effect on the excessive accumulation of ROS or the mitochondrial membrane potential loss (Fig S6A-E). Collectively, these data identify that lapatinib may induce DNA damage and keratinocyte apoptosis by downregulating HMGB1 expression, and HMGB1 might be a reliable target for treating the cutaneous toxicity of lapatinib.

Saikosaponin A mitigates lapatinib-induced cutaneous toxicity by recovering HMGB1 expression.

Based on the results thus far, we speculated that pharmacological recover HMGB1 expression could be a potential strategy against lapatinib-induced cutaneous toxicity. Therefore, we initially screened the natural product library to seek for the potential strategy for the treatment of lapatinib-induced cutaneous toxicity that could recover the expression of HMGB1. To our delight, saikosaponin A could significantly improve the transcription level of *HMGB1* (Fig. 7A). Hence, we hypothesized that saikosaponin A could alleviate cutaneous toxicity caused by lapatinib via recovering HMGB1 expression level. To prove it, we examined HMGB1 mRNA and protein levels in keratinocytes exposed to lapatinib with or without saikosaponin A. As shown in Fig. 7B-D, lapatinib treatment significantly decreased the mRNA and protein levels of HMGB1. Under saikosaponin A co-treatment, the mRNA and protein levels of HMGB1 recovered to normal level. Next, we further verified whether saikosaponin A could mitigate lapatinib-induced DNA damage and apoptosis in keratinocytes. Results showed that saikosaponin A could reduce the length and intensity of the comet tail caused by lapatinib, signifying the alleviation of DNA breaks (Fig. 7E, F). Consistently, saikosaponin A significantly reversed lapatinib-induced upregulation of G-H2A.X protein

levels (Fig. 7G-I). We also observed that under the co-treatment of saikosaponin A, the upregulation of c-PARP and c-CASP3 protein levels was inhibited (Fig. 7J, K). The flow cytometry results presented the same finding, indicating that saikosaponin A could inhibit the apoptosis of keratinocytes induced by lapatinib (Fig. 7L, M). Further investigation of the effect of saikosaponin A on lapatinib-induced keratinocyte death showed that saikosaponin A could improve the survival fraction of keratinocytes even under lapatinib treatment (Fig. 8N). All these results suggested that saikosaponin A could protect keratinocytes from lapatinib-induced cutaneous toxicity *in vitro*.

To further evaluate the therapeutic effect of saikosaponin A on lapatinib-induced cutaneous toxicity *in vivo*, we developed an animal model treated with lapatinib (950 mg/kg) at the absence or presence of saikosaponin A (20 mg/kg) for 28 days. It was gratifying that saikosaponin A could obviously mitigate lapatinib-induced generalized xerosis and scales (Fig. 8A, B). H&E staining results showed that epidermal edema and nuclear pyknosis of keratinocytes in the abdominal skin tissue of lapatinib-treated mice were significantly alleviated by saikosaponin A. Meanwhile, the epidermal thickness returned to the normal level (Fig. 8C, D). The combination of saikosaponin A could significantly downregulate the increased level of TNFA induced by lapatinib (Fig. 8E). Furthermore, the epidermic tissue of mice treated with both saikosaponin A and lapatinib showed a significant decrease in the number of TUNEL-positive (green fluorescence) keratinocytes, which demonstrated that saikosaponin A could significantly inhibit the apoptosis of keratinocytes induced by lapatinib *in vivo* (Fig. 8F, G).

We then turned to determine the relevance of HMGB1 expression upregulation to the therapeutic effect of saikosaponin A against lapatinib-induced cutaneous toxicity *in vivo*. In line with our expected results, the level of HMGB1 protein in skin tissue of mice treated with lapatinib alone was significantly downregulated, while saikosaponin A could reverse this effect (Fig. 8H, I). In conclusion, these results reveal that saikosaponin A plays a protective role in lapatinib-induced cutaneous toxicity by upregulating HMGB1 expression, which therefore could be a promising clinical treatment to combat lapatinib-induced cutaneous toxicity.

Discussion

As the first line of defense against infection and injury, skin provides body with the protection from the external environment, as well as regulates the body temperature, metabolism and sensory capabilities (Gravitz, 2018). Cutaneous toxicity is the side effect of certain drugs on skin, which is often observed in patients treated with EGFR inhibitors including lapatinib. The clinical manifestations of lapatinib-induced cutaneous toxicity mainly include rash, generalized xerosis and pruritus (Morita, Iizuka-Ohashi et al., 2021). Severe cutaneous toxicity could cause a reduction in the dosage or even withdrawal, eventually worsen the survival quality and psychological health of patients. Therefore, it's urgent to investigate detailed mechanism and develop corresponding intervention strategies to avoid effect of cutaneous toxicity on treatment efficacy.

To mimic the occurrence of cutaneous toxicity during lapatinib treatment in clinic, we converted the clinical human dose of lapatinib into the animal dose in proportion and treated the mice with 950 mg/kg lapatinib daily for 28 days. Consistent with clinical manifestations, we observed that almost all (12 of 14) mice treated with lapatinib exhibited progressive xerosis and serve desquamation. Furthermore, we found that the skin tissue of the mice showed severe damage mainly manifested as significant thickening of the epidermal layer, intracellular edema and nuclear pyknosis of keratinocytes. The above results showed that lapatinib could indeed cause cutaneous toxicity in mice. In addition, we found that lapatinib treatment apparently decreased cytokeratin 5, a marker of keratinocyte in mouse skin. As the main constituent of epidermis, keratinocytes serve as skin barrier and it is maintained by a tightly controlled balance between the proliferation and differentiation (Wilson, 2014). Under normal condition, keratinocytes proliferate continually at the basal lamina and differentiate towards the skin surface (Laksono, Fortugno et al., 2020). In this process, their characteristics change significantly and show different physiological functions in epidermis, such as promoting the renewal of epidermal layer and resisting external pathogens (Fuchs & Horsley, 2008). Conversely, disorders of keratinocytes play a vital role in skin pathology process. The occurrence of psoriasis is related to the hyper-proliferation of keratinocytes and sorafenib-induced severe hand-foot skin reaction was caused by keratinocyte over-differentiation (Furue, Furue et al., 2020, Lane, Rugg et al., 1992, Luo et al., 2020). In our study, the loss of keratinocytes in the skin of lapatinib-treated mice might be the key reason for lapatinib-induced cutaneous toxicity.

Cytokeratin is produced by keratinocytes during differentiation, which serves as structural and mechanical support. In addition, keratin also regulates the growth, adhesion, migration and invasion of epithelial cells. Therefore, the dysfunction or mutation of keratin is related to a variety of skin diseases (Knobel, O'Toole et al., 2015). It is reported that cytokeratin 5, a member of intermediate filament protein family, whose mutations is associated with epidermolysis bullosa simplex (EBS) (Knobel et al., 2015, Lane et al., 1992). Consistently, we found the expression of cytokeratin 5 was notably decreased in epidermis under lapatinib treatment, indicating the latent role of cytokeratin 5 in skin disorders caused by lapatinib.

In innate immune response, cytokeratin is also considered as the gatekeeper in both local and systemic inflammation. Under wounding or psoriasis pathogenesis, cytokeratin 6, 16 and 17 in the skin will be triggered by the innate immune system of keratinocytes and increase rapidly (Zhang, Yin et al., 2019). Conversely, cytokeratin 1 deficient mice exhibit a striking inflammatory disease phenotype with skin specific and systemic components (Mukai, Tsai et al., 2018). Therefore, the role of keratin could be the "generator" of inflammation or the harmful "effector". In our study, we observed mRNA level of pro-inflammatory factors *TNFA, IL6, IL18* and chemokine factor *CCL2* were increased in keratinocytes upon lapatinib treatment. To be noticed, we observed the increased IL6 level instead of TNFA, in the medium of lapatinib-treated keratinocytes. Several studies reported that IL6, CCL2 and IL18 are key factors in the activation of mast cells (Collington, Hallgren et al., 2010, Desai, Jung et al., 2016, Wiener, Pocza et al., 2008), and mast cells can not only activate endothelial cells and attract neutrophils, which is the key event of many acute inflammatory reactions, but also release inflammatory factor TNFA in the process of

inflammatory reaction in response to particular immune or non-immune stimuli (Gibbs, Wierecky et al., 2001). Indeed, we found the presence of hyperchromatic mast cells in the epidermis of the lapatinib-treated mice, which might explain why TNFA increased in mouse serum, but not in cell medium. This preliminary finding indicated the inflammatory transformation of keratinocytes, which is yet to be confirmed by single-cell RNA sequencing.

It has been well known that inhibition of EGFR could cause severe skin damage (Lichtenberger, Gerber et al., 2013). However, from the perspective of the correlation between the therapeutic effect of lapatinib and cutaneous toxicity, it is still controversial whether the cutaneous toxicity induced by lapatinib is related to targets inhibition (Kaya, Gumus et al., 2016). Moreover, there is no evidence that the cutaneous toxicity associated with lapatinib treatment can predict the prognosis of breast cancer thus far. Here, we found that knockdown/overexpression of *ERBB2* or *EGFR* had no significant effect on lapatinib-induced keratinocyte mortality, suggesting that lapatinib-induced cutaneous toxicity might be independent on the inhibition of its targets. Moreover, our RNA-Seq data revealed that lapatinib could induce mitochondrial dysfunction, DNA damage and innate immune response in keratinocytes. To identify the key regulator of lapatinib-induced cutaneous toxicity, we analyzed the overlap of differentially expressed genes from GO terms of DNA repair, cellular response to DNA damage and innate immune response and identified HMGB1 as the candidate regulator. Intracellular HMGB1 acts as a DNA chaperone with the ability of binding to DNA and promoting its bending, in turn exerts essential role in regulating DNA activities (Kang et al., 2014). However, the transcriptional level of HMGB1 in keratinocyte was decreased by lapatinib in a time and dose-dependent manner. However, whether HMGB1 directly regulates the expression of genes related to DNA damage and repair has not been fully clarified. The chromatin immunoprecipitation assay could be used to answer the question but the incompatibility of standard formaldehyde fixation with HMG box DNA binding domain contributes to the challenge of capturing HMGB protein on chromatin, which is yet to be solved by new technology (Sofiadis, Josipovic et al., 2021).

We found that the release of HMGB1 from the supernatant of lapatinib-administrated HaCaT cells was nearly undetectable, which indicate that intracellular rather than extracellular HMGB1 is involved in lapatinib induced cutaneous toxicity. It has been reported that nuclear HMGB1-mediated chromatin remodeling can affect IL24 expression, suggesting that nuclear HMGB1 also plays an important role in the pathological progression of skin immune process (Kang et al., 2011). Consistent with the assumption, overexpression of HMGB1 could inhibit the expression of inflammatory factors. Therefore, we speculate that HMGB1 may play a role in the regulation of skin immune homeostasis by regulating the transcription level of inflammatory factors, and the specific regulatory process needs to be further confirmed.

The confirmation that lapatinib induced cutaneous toxicity via inhibiting the expression of HMGB1 promoted us to seek for the compound that could recover the expression of HMGB1 and rescue the skin injury. Delightfully, we found the candidate compound saikosaponin A through screening. Saikosaponin A, a triterpenoid glycoside extracted from *Bupleurum chinensis* DC, exerts multiple pharmacological activities including anti-inflammatory, anti-oxidant and immunity regulatory abilities (Fu, Hu et al., 2015). Unfortunately, the precise mechanism underlying the regulation of HMGB1 transcription by saikosaponin

A is still unknown. We will use saikosaponin A as a probe to clarify the regulation of HMGB1 transcription during DNA damage and inflammatory response in future study. Here, we found that combination of saikosaponin A could inhibit lapatinib-induced DNA damage, keratinocyte apoptosis and alleviate immune response, further preventing the cutaneous toxicity in mice caused by lapatinib. Moreover, saikosaponin A possesses the ability to inhibit proliferation and metastasis of breast cancer cells to effectively arrest the development of breast cancer (Wang, Zhao et al., 2019), suggesting that saikosaponin A combined with lapatinib could be a better strategy for the treatment of breast cancer via reducing toxicity and enhancing efficacy.

Conclusions

In summary, the data presented in this study provided an insight into the understanding of lapatinib-promoted cutaneous toxicity wherein lapatinib induces mitochondrial dysfunction, causes DNA damage and finally results in apoptosis of keratinocytes. In addition, we further confirmed that decreased HMGB1 expression contributes to the occurrence of the toxicity. More importantly, based on the mechanistic findings, a potentially valuable therapeutic regimen is identified, which may not only bring new hope to patients under lapatinib-based cancer treatment, but also shed new light on the intervention of cutaneous adverse drug reactions induced by other EGFR or ERBB2 inhibitors.

Abbreviations

CPT, Camptothecin; DMSO, Dimethyl sulfoxide; EDTA, Ethylenediaminetetraacetic acid; FBS, Fetal bovine serum; LAPA, lapatinib; NF-κB, Nuclear factor-κB; PBS, Phosphate buffered saline; ROS, Reactive oxygen species; TNFA, Tumour necrosis factor-α; Tris, 2-amino-2-hydroxymethylpropan-1,3,-diol; SD, Standard deviation (of observed sample); SDS-PAGE, Sodium dodecyl sulphate-polyacrylamide gel electrophoresis; SSA, Saikosaponin a; TUNEL, Terminal deoxynucleotidyl transferase dUTP nick end labeling.

Declarations

Author contributions Liyu Jiang and Yan Zeng investigated, conducted experiments, acquired and analyzed data, created the figures and wrote the manuscript. Leilei Ai investigated, wrote original draft, provided funding and reviewed the manuscript. Xiaochun Yang, Bo Yang and Hao Yan analyzed data and reviewed the manuscript. Peihua Luo acquired and analyzed data and provided funding. Qiaojun He conceived the project, designed the experiments and reviewed the manuscript. Zhifei Xu conceived the project, designed the experiments, reviewed the manuscript and provided funding.

Acknowledgments The authors thank anyone who contributed to the article. We would also like to thank experimenter Wei Yin from Image Center, Core Facilities, School of Medicine, Zhejiang University for the confocal laser scanning microscope images.

Funding This work was supported by National Natural Science Foundation of China (No. 81872941 and No. 82003862), Postdoctoral Foundation of Zhejiang Province (No. ZJ2020038) and the Fundamental Research Funds for the Central Universities, China, Innovation research grant program for 8-year-system medical students at Zhejiang University (No. 119000-5405A1).

Data availability The datasets generated during and/or analyzed during the current study are availablein the Gene Expression Omnibus repository (https://www.ncbi.nlm.nih.gov/geo/query/acc.cgi?acc=GSE195713).

Competing interests The authors declare no competing interests.

Ethics approval The experimental procedures involved in animal experiments were approved by the Zhejiang University Animal Care and Use Committee, and applicable institutional and governmental regulations concerning the ethical use of animals were followed.

References

1. Atkinson SD, McGilligan VE, Liao H, Szeverenyi I, Smith FJ, Moore CB , et al. Development of allele-specific therapeutic siRNA for keratin 5 mutations in epidermolysis bullosa simplex. *J Invest Dermatol* 2011:(131): 2079-2086.https://doi.org/10.1038/jid.2011.169.
2. Balkwill F TNF-alpha in promotion and progression of cancer. *Cancer Metastasis Rev* 2006:(25): 409-416.https://doi.org/10.1007/s10555-006-9005-3.
3. Carr DF, Wang CW, Bellon T, Ressel L, Nwikue G, Shrivastava V , et al. Serum and blister-fluid elevation and decreased epidermal content of high-mobility group box 1 protein in drug-induced Stevens-Johnson syndrome/toxic epidermal necrolysis. *Br J Dermatol* 2019:(181): 166-174.https://doi.org/10.1111/bjd.17610.
4. Chen M, Chen J, Peng X, Xu Z, Shao J, Zhu Y , et al. The contribution of keratinocytes in capecitabine-stimulated hand-foot-syndrome. *Environ Toxicol Pharmacol* 2017:(49): 81-88.https://doi.org/10.1016/j.etap.2016.12.001.
5. Circu ML, Aw TY Reactive oxygen species, cellular redox systems, and apoptosis. *Free Radic Biol Med* 2010:(48): 749-762.https://doi.org/10.1016/j.freeradbiomed.2009.12.022.
6. Collington SJ, Hallgren J, Pease JE, Jones TG, Rollins BJ, Westwick J , et al. The role of the CCL2/CCR2 axis in mouse mast cell migration in vitro and in vivo. *J Immunol* 2010:(184): 6114-6123.https://doi.org/10.4049/jimmunol.0904177.
7. Desai A, Jung MY, Olivera A, Gilfillan AM, Prussin C, Kirshenbaum AS , et al. IL-6 promotes an increase in human mast cell numbers and reactivity through suppression of suppressor of cytokine signaling 3. *J Allergy Clin Immunol* 2016:(137): 1863-1871 e1866.https://doi.org/10.1016/j.jaci.2015.09.059.
8. Ergen EN, Hughey LC Stevens-Johnson Syndrome and Toxic Epidermal Necrolysis. *JAMA Dermatol* 2017:(153): 1344.https://doi.org/10.1001/jamadermatol.2017.3957.

9. Fabbrocini G, Panariello L, Caro G, Cacciapuoti S Acneiform Rash Induced by EGFR Inhibitors: Review of the Literature and New Insights. *Skin Appendage Disord* 2015:(1): 31-37.https://doi.org/10.1159/000371821.
10. Friedman MD, Lacouture M, Dang C Dermatologic Adverse Events Associated With Use of Adjuvant Lapatinib in Combination With Paclitaxel and Trastuzumab for HER2-Positive Breast Cancer: A Case Series Analysis. *Clin Breast Cancer* 2016:(16): e69-74.https://doi.org/10.1016/j.clbc.2015.11.001.
11. Fu Y, Hu X, Cao Y, Zhang Z, Zhang N Saikosaponin a inhibits lipopolysaccharide-oxidative stress and inflammation in Human umbilical vein endothelial cells via preventing TLR4 translocation into lipid rafts. *Free Radic Biol Med* 2015:(89): 777-785.https://doi.org/10.1016/j.freeradbiomed.2015.10.407.
12. Fuchs E, Horsley V More than one way to skin. *Genes Dev* 2008:(22): 976-985. https://doi.org/10.1101/gad.1645908.
13. Furue M, Furue K, Tsuji G, Nakahara T Interleukin-17A and Keratinocytes in Psoriasis. *Int J Mol Sci* 2020:(21)https://doi.org/10.3390/ijms21041275.
14. Gibbs BF, Wierecky J, Welker P, Henz BM, Wolff HH, Grabbe J Human skin mast cells rapidly release preformed and newly generated TNF-alpha and IL-8 following stimulation with anti-IgE and other secretagogues. *Exp Dermatol* 2001:(10): 312-320.https://doi.org/10.1034/j.1600-0625.2001.100503.x.
15. Gravitz L Skin. *Nature* 2018:(563): S83.https://doi.org/10.1038/d41586-018-07428-4.
16. Hoetzenecker W, Nageli M, Mehra ET, Jensen AN, Saulite I, Schmid-Grendelmeier P , et al. Adverse cutaneous drug eruptions: current understanding. *SeminImmunopathol* 2016:(38): 75-86.https://doi.org/10.1007/s00281-015-0540-2.
17. Jin Y, Chen X, Gao Z, Shen X, Fu H, Pan Z , et al. Bisdemethoxycurcumin alleviates vandetanib-induced cutaneous toxicity in vivo and in vitro through autophagy activation. *Biomed Pharmacother* 2021:(144): 112297.https://doi.org/10.1016/j.biopha.2021.112297.
18. Kang R, Chen R, Zhang Q, Hou W, Wu S, Cao L , et al. HMGB1 in health and disease. *Mol Aspects Med* 2014:(40): 1-116.https://doi.org/10.1016/j.mam.2014.05.001.
19. Kang R, Livesey KM, Zeh HJ, 3rd, Lotze MT, Tang D Metabolic regulation by HMGB1-mediated autophagy and mitophagy. *Autophagy* 2011:(7): 1256-1258.https://doi.org/10.4161/auto.7.10.16753.
20. Kaya S, Gumus M, Gurbuz Y, Cabuk D, Acikgoz O, Temiz S , et al. The prognostic value of beta-catenin and LEF-1 expression in patients with operable gastric carcinoma. *Am J Transl Res* 2016:(8): 1228-1236.
21. Knobel M, O'Toole EA, Smith FJ Keratins and skin disease. *Cell Tissue Res* 2015:(360): 583-589.https://doi.org/10.1007/s00441-014-2105-4.
22. Kuo LJ, Yang LX Gamma-H2AX - a novel biomarker for DNA double-strand breaks. *In Vivo* 2008:(22): 305-309.
23. Laksono BM, Fortugno P, Nijmeijer BM, de Vries RD, Cordisco S, Kuiken T , et al. Measles skin rash: Infection of lymphoid and myeloid cells in the dermis precedes viral dissemination to the epidermis.

PLoS Pathog 2020:(16): e1008253.https://doi.org/10.1371/journal.ppat.1008253.

24. Lane EB, Rugg EL, Navsaria H, Leigh IM, Heagerty AH, Ishida-Yamamoto A , et al. A mutation in the conserved helix termination peptide of keratin 5 in hereditary skin blistering. *Nature* 1992:(356): 244-246.https://doi.org/10.1038/356244a0.
25. Lichtenberger BM, Gerber PA, Holcmann M, Buhren BA, Amberg N, Smolle V , et al. Epidermal EGFR controls cutaneous host defense and prevents inflammation. *Sci Transl Med* 2013:(5): 199ra111.https://doi.org/10.1126/scitranslmed.3005886.
26. Liu S, Kurzrock R Toxicity of targeted therapy: Implications for response and impact of genetic polymorphisms. *Cancer Treat Rev* 2014:(40): 883-891.https://doi.org/10.1016/j.ctrv.2014.05.003.
27. Luo P, Yan H, Chen X, Zhang Y, Zhao Z, Cao J , et al. s-HBEGF/SIRT1 circuit-dictated crosstalk between vascular endothelial cells and keratinocytes mediates sorafenib-induced hand-foot skin reaction that can be reversed by nicotinamide. *Cell Res* 2020:(30): 779-793.https://doi.org/10.1038/s41422-020-0309-6.
28. Luo P, Yan H, Du J, Chen X, Shao J, Zhang Y , et al. PLK1 (polo like kinase 1)-dependent autophagy facilitates gefitinib-induced hepatotoxicity by degrading COX6A1 (cytochrome c oxidase subunit 6A1). *Autophagy* 2021:(17): 3221-3237.https://doi.org/10.1080/15548627.2020.1851492.
29. Ly JD, Grubb DR, Lawen A The mitochondrial membrane potential (deltapsi(m)) in apoptosis; an update. *Apoptosis* 2003:(8): 115-128.https://doi.org/10.1023/a:1022945107762.
30. Macdonald JB, Macdonald B, Golitz LE, LoRusso P, Sekulic A Cutaneous adverse effects of targeted therapies: Part I: Inhibitors of the cellular membrane. *J Am Acad Dermatol* 2015:(72): 203-218; quiz 219-220.https://doi.org/10.1016/j.jaad.2014.07.032.
31. Medeiros B, Allan AL Molecular Mechanisms of Breast Cancer Metastasis to the Lung: Clinical and Experimental Perspectives. *Int J Mol Sci* 2019:(20)https://doi.org/10.3390/ijms20092272.
32. Moreira C, Kaklamani V Lapatinib and breast cancer: current indications and outlook for the future. *Expert Rev Anticancer Ther* 2010:(10): 1171-1182.https://doi.org/10.1586/era.10.113.
33. Morita M, Iizuka-Ohashi M, Watanabe M, Narita T, Kato C, Kakibuchi D , et al. *J Clin Biochem Nutr* 2021:(68): 235-242.https://doi.org/10.3164/jcbn.20-112.
34. Mou K, Liu W, Han D, Li P HMGB1/RAGE axis promotes autophagy and protects keratinocytes from ultraviolet radiation-induced cell death. *J Dermatol Sci* 2017:(85): 162-169.https://doi.org/10.1016/j.jdermsci.2016.12.011.
35. Mukai K, Tsai M, Saito H, Galli SJ Mast cells as sources of cytokines, chemokines, and growth factors. *Immunol Rev* 2018:(282): 121-150.https://doi.org/10.1111/imr.12634.
36. Nadanaciva S, Will Y Current concepts in drug-induced mitochondrial toxicity. *Current protocols in toxicology* 2009:(Chapter 2): Unit 2 15.https://doi.org/10.1002/0471140856.tx0215s40.
37. Onishi Y, Tanimoto Y, Kizaki H Inflammation and apoptosis. *Bull Tokyo Dent Coll* 1997:(38): 65-76.
38. Ramirez A, Bravo A, Jorcano JL, Vidal M Sequences 5' of the bovine keratin 5 gene direct tissue- and cell-type-specific expression of a lacZ gene in the adult and during development. *Differentiation*

1994:(58): 53-64.https://doi.org/10.1046/j.1432-0436.1994.5810053.x.

39. Senda N, Yanai H, Hibino S, Li L, Mizushima Y, Miyagaki T , et al. HMGB1-mediated chromatin remodeling attenuates Il24 gene expression for the protection from allergic contact dermatitis. *Proc Natl Acad Sci U S A* 2021:(118)https://doi.org/10.1073/pnas.2022343118.
40. Simpson CL, Patel DM, Green KJ Deconstructing the skin: cytoarchitectural determinants of epidermal morphogenesis. *Nat Rev Mol Cell Biol* 2011:(12): 565-580.https://doi.org/10.1038/nrm3175.
41. Sofiadis K, Josipovic N, Nikolic M, Kargapolova Y, Ubelmesser N, Varamogianni-Mamatsi V , et al. HMGB1 coordinates SASP-related chromatin folding and RNA homeostasis on the path to senescence. *Mol Syst Biol* 2021:(17): e9760.https://doi.org/10.15252/msb.20209760.
42. Sonnenblick A, de Azambuja E, Agbor-Tarh D, Bradbury I, Campbell C, Huang Y , et al. Lapatinib-Related Rash and Breast Cancer Outcome in the ALTTO Phase III Randomized Trial. *J Natl Cancer Inst* 2016:(108)https://doi.org/10.1093/jnci/djw037.
43. Tang Y, Tu H, Liu G, Zheng G, Wang M, Li L , et al. RNF31 Regulates Skin Homeostasis by Protecting Epidermal Keratinocytes from Cell Death. *J Immunol* 2018:(200): 4117-4124.https://doi.org/10.4049/jimmunol.1800172.
44. Tischer B, Huber R, Kraemer M, Lacouture ME Dermatologic events from EGFR inhibitors: the issue of the missing patient voice. *Support Care Cancer* 2017:(25): 651-660.https://doi.org/10.1007/s00520-016-3419-4.
45. Van Opdenbosch N, Lamkanfi M Caspases in Cell Death, Inflammation, and Disease. *Immunity* 2019:(50): 1352-1364.https://doi.org/10.1016/j.immuni.2019.05.020.
46. Wang Y, Zhao L, Han X, Wang Y, Mi J, Wang C , et al. Saikosaponin A Inhibits Triple-Negative Breast Cancer Growth and Metastasis Through Downregulation of CXCR4. *Front Oncol* 2019:(9): 1487.https://doi.org/10.3389/fonc.2019.01487.
47. Wiener Z, Pocza P, Racz M, Nagy G, Tolgyesi G, Molnar V , et al. IL-18 induces a marked gene expression profile change and increased Ccl1 (I-309) production in mouse mucosal mast cell homologs. *Int Immunol* 2008:(20): 1565-1573.https://doi.org/10.1093/intimm/dxn115.
48. Wilson VG Growth and differentiation of HaCaT keratinocytes. *Methods Mol Biol* 2014:(1195): 33-41.https://doi.org/10.1007/7651_2013_42.
49. Xu Z, Jin Y, Yan H, Gao Z, Xu B, Yang B , et al. High-mobility group box 1 protein-mediated necroptosis contributes to dasatinib-induced cardiotoxicity. *Toxicol Lett* 2018:(296): 39-47.https://doi.org/10.1016/j.toxlet.2018.08.003.
50. Zhang C, Zhu Z, Gao J, Yang L, Dang E, Fang H , et al. Plasma exosomal miR-375-3p regulates mitochondria-dependent keratinocyte apoptosis by targeting XIAP in severe drug-induced skin reactions. *Sci Transl Med* 2020:(12)https://doi.org/10.1126/scitranslmed.aaw6142.
51. Zhang X, Yin M, Zhang LJ Keratin 6, 16 and 17-Critical Barrier Alarmin Molecules in Skin Wounds and Psoriasis. *Cells* 2019:(8)https://doi.org/10.3390/cells8080807.

52. Zhu X, Messer JS, Wang Y, Lin F, Cham CM, Chang J , et al. Cytosolic HMGB1 controls the cellular autophagy/apoptosis checkpoint during inflammation. *J Clin Invest* 2015:(125): 1098-1110.https://doi.org/10.1172/JCI76344.

Figures

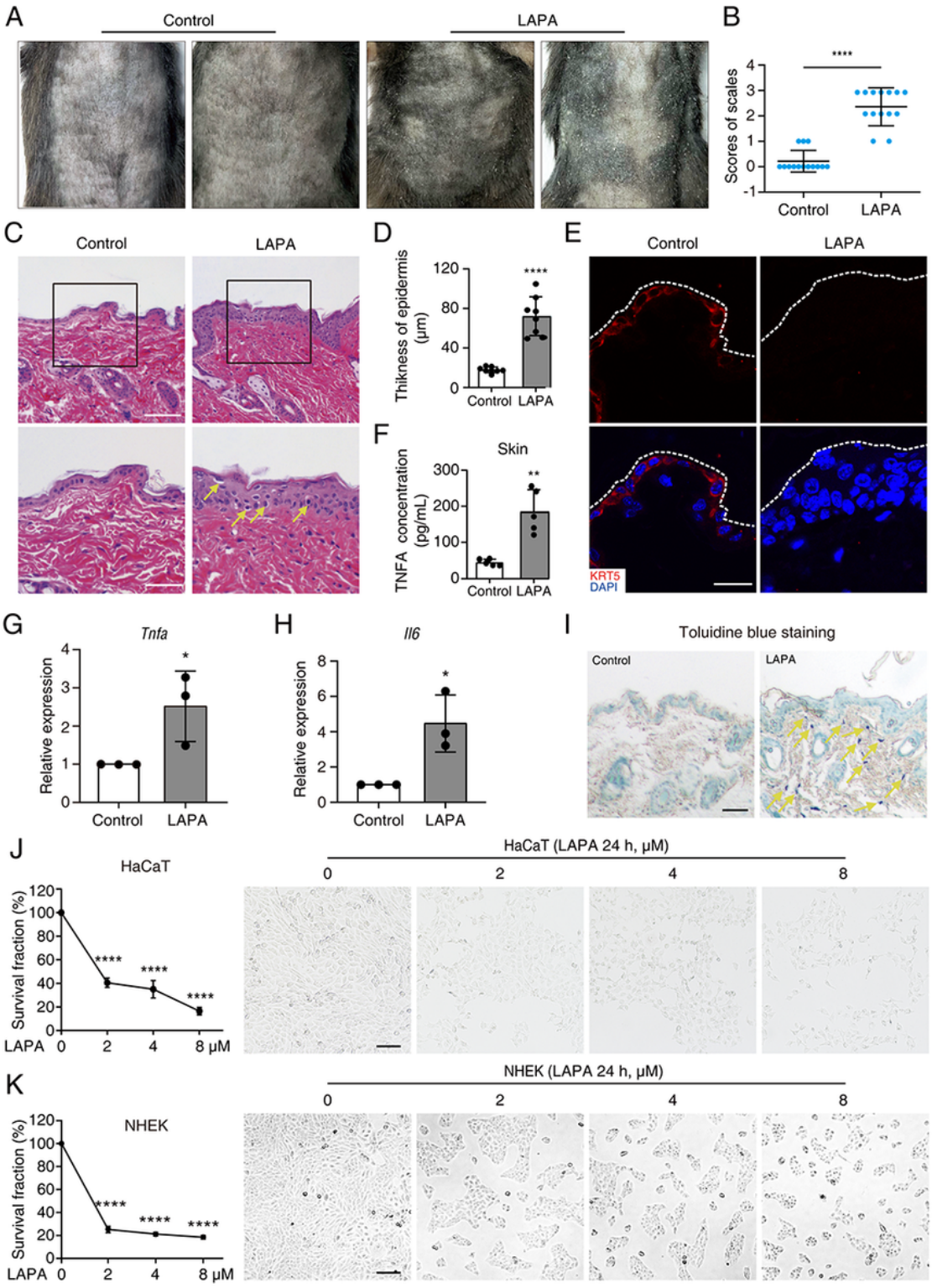

Figure 1

Lapatinib causes cutaneous toxicity in mice and cell death in human keratinocytes. (A-G) C57BL/6 mice were administered with 0.5% CMC-Na or lapatinib (950 mg/kg) for 28 days, skin tissues were harvested after mice were sacrificed. **A** Representative images of scales induced by lapatinib in mice. **B** Scales of the abdominal skin in mice was scored on a scale from 0 to 3, which was divided into four grades: none, light, moderate and severe according to the clinical manifestation criteria. **C, D** Microscope images of H&E staining performed on the stratum corneum of the mice. **C** Upper and lower panels showing lower and higher magnification of the skin tissues in mice with H&E staining, respectively. Scale bars: 50 μm, 25 μm. **D** Quantitative analysis of thickness of epidermal layer (n = 8). **E** Immunofluorescence assay showing the expression of keratinocyte marker cytokeratin 5 in mouse epidermis. Scale bars: 20 μm. **F** The secretory level of TNFA in mice serum was analyzed by ELISA assay. **G, H** The mRNA levels of *TNFA* and *Il6* in skin tissue of mice were analyzed by RT-qPCR. **I** Toluidine blue staining of skin showed deep violet/mazarine colored (indicated by yellow arrow) mast cells. Scale bars: 25 μm. **J, K** Cell survival fraction of HaCaT cells and NHEK cells treated with 0, 2, 4 and 8 μM lapatinib for 24 h was detected by SRB assay. The morphology of the cells was obtained by microscope. Scale bars: 50 μm. Three independent experiments were performed and the data were shown as Mean ± SD. The P value was calculated by Student's t test (unpaired, two-tailed, 2 groups). *P < 0.05. LAPA, lapatinib. Statistical significance was assessed using 2-tailed Student's t test or one-way ANOVA (Dunnett's multiple comparisons test). **P < 0.01; ***P < 0.001; ****P < 0.0001.

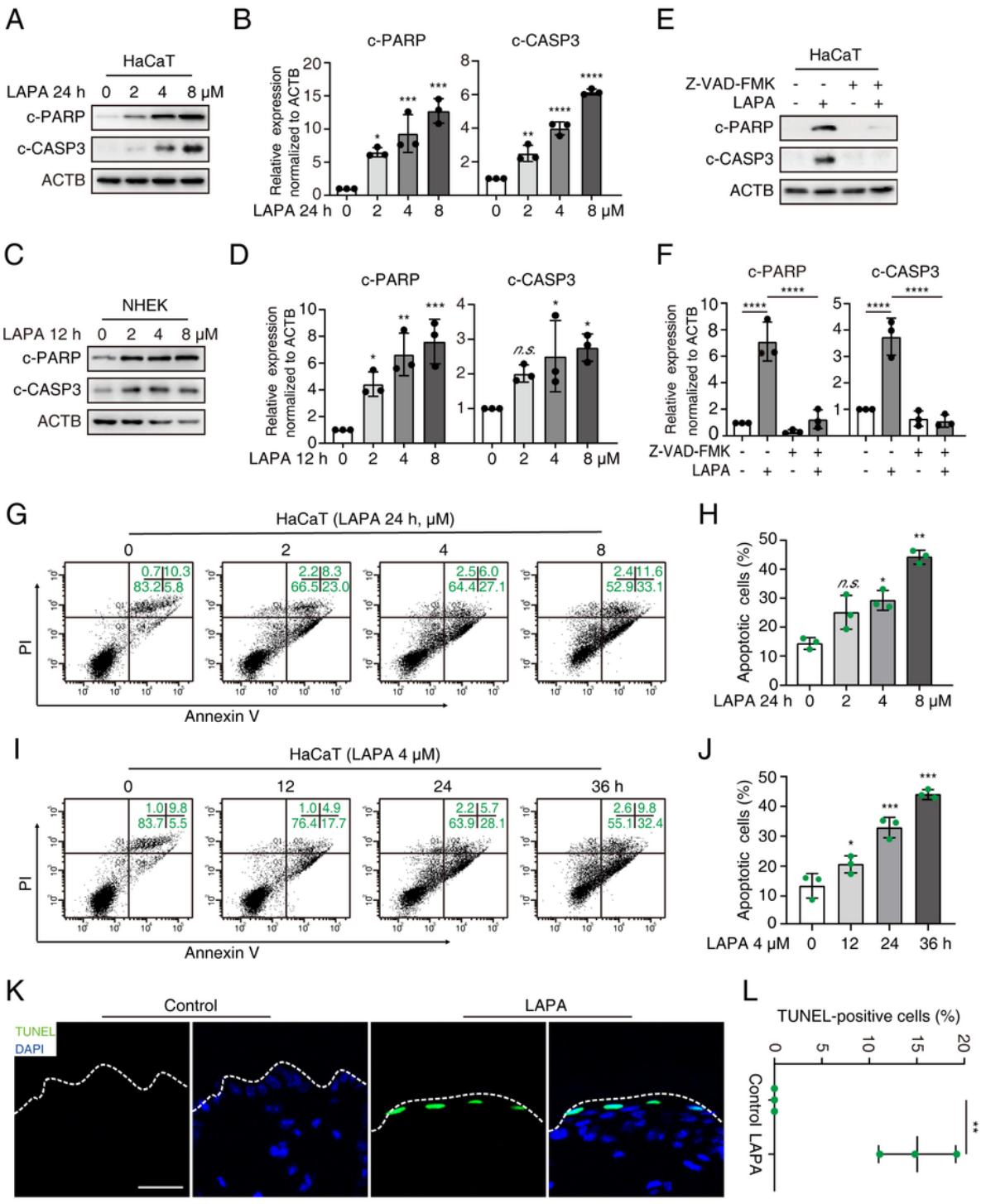

Figure 2

Lapatinib activates apoptotic signal in human keratinocytes. **A-D** HaCaT cells and NHEK cells were treated with 0, 2, 4 and 8 μM lapatinib for 24 h, and the protein levels of c-PARP and c-CASP3 were analyzed by western blot using ACTB as a loading control. Densitometric analysis was carried out. **E, F** HaCaT cells treated with Z-VAD-FMK (20 μM) or/and lapatinib (4 μM) for 24 h, then the protein levels of c-PARP and c-CASP3 were detected by western blot using ACTB as a loading control. Densitometric

analysis was carried out. **G-J** HaCaT cells were treated with lapatinib for indicated concentrations and time. Flow cytometry stained with PI/Annexin V was used to measure the apoptosis rates, and representative images were shown. **K, L** Fluorescence microscope images of keratinocytes stained with TUNEL and DAPI of mouse skin tissue. The number of TUNEL-positive dots were calculated. Scale bars: 100 μm. Three independent experiments were performed and the data were shown as Mean ± SD. The *P* value was calculated by Student's *t* test (unpaired, two-tailed, 2 groups) or by one-way ANOVA (Dunnett's multiple comparisons test or Sidak test). *n.s.*, no significance; **P* < 0.05; ***P* < 0.01; ****P* < 0.001; *****P* < 0.0001.

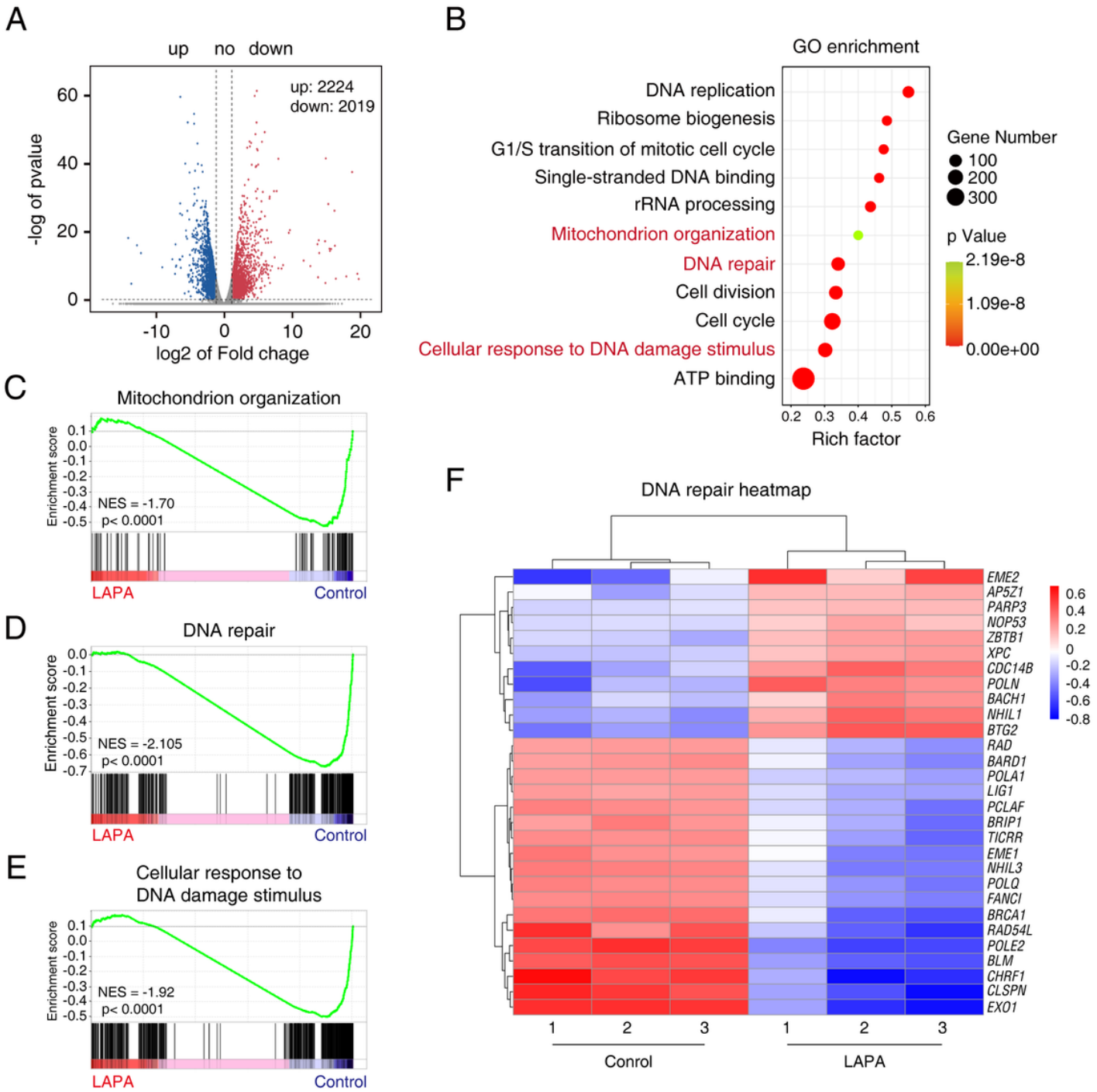

Figure 3

RNA-Seq analysis reveals that lapatinib-induced keratinocyte apoptosis is related to mitochondrial dysfunction and DNA damage. HaCaT cells were treated with or without 4 μM lapatinib and performed with RNA-Seq analysis. **A** Volcano map of differentially expressed genes between the control and lapatinib administration group. The red dots represented significantly downregulated genes, while the blue dots represented significantly upregulated genes. **B** Significant enriched GO terms between the control and lapatinib-treated group based on their functions. **C-E** GSEA for mitochondrion organization, DNA damage and repair gene sets enriched in the lapatinib-treated group *vs.* the control. **F** Heatmap showing fold changes of the selected genes in lapatinib-treated group compared with the control.

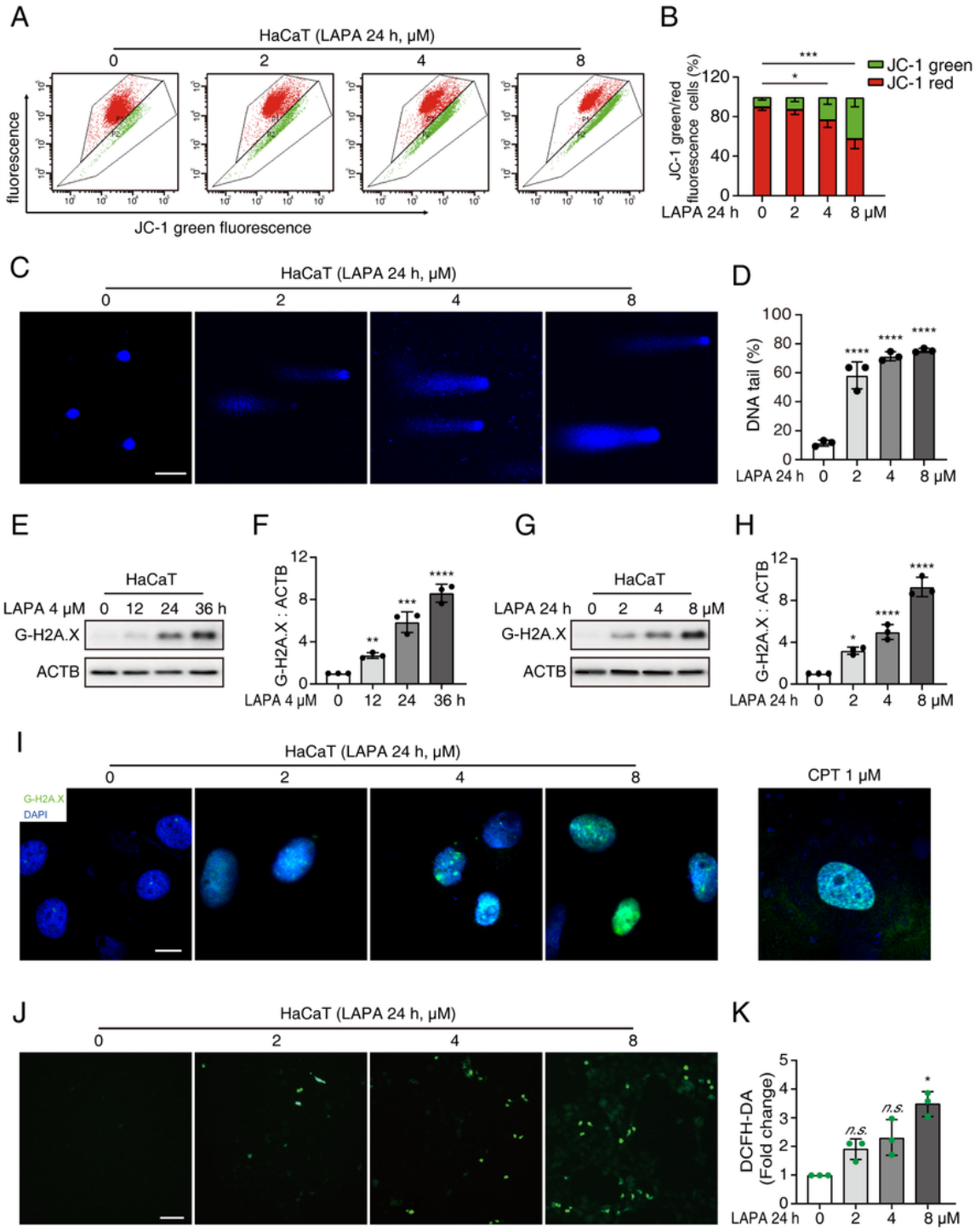

Figure 4

DNA damage is involved in lapatinib-induced keratinocyte apoptosis. **A** Flow cytometry with JC-1 staining was used to analyze the loss of mitochondrial membrane potential in HaCaT cells treated with 0, 2, 4 and 8 μM lapatinib for 24 h. **B** Quantitative analysis of cells with J-aggregates (red) or monomers (green) after the administration of lapatinib. **C, D** Typical images of DNA damage after lapatinib treatment detected by comet assay. Quantitative analysis was performed on the percentage of DNA tail. The

statistical analysis of comet assay was performed using one-way ANOVA, *n* = 50 cells per group. Scale bars: 100 μm. **E-H** Representative immunoblots of G-H2A.X protein in HaCaT cells stimulated with lapatinib. Densitometric analysis was carried out. **E, F** HaCaT cells was treated with 4 μM lapatinib for 0, 12, 24 and 36 h. **G, H** HaCaT cells treated with 0, 2, 4 and 8 μM lapatinib for 24 h. **I** Immunofluorescence assay was performed in HaCaT cells by detecting the protein level of G-H2A.X, using CPT as a positive control. **J, K** HaCaT cells were treated with 0, 2, 4 and 8 μM lapatinib for 24 h followed by DCFH-DA staining. The representative images of intracellular ROS were shown. Scale bars: 100 μm. The level of intracellular ROS was analyzed by flow cytometry. Three independent experiments were performed and the data were shown as Mean ± SD. The *P* value was calculated by one-way ANOVA (Dunnett's multiple comparisons test or Sidak test). *n.s.*, no significance; **P* < 0.05; ***P* < 0.01; ****P* < 0.001, *****P* < 0.0001.

Figure 5

Lapatinib induces aberrant immune response in keratinocytes. **A** HaCaT cells were treated with or without 4 μM lapatinib and performed with RNA-Seq analysis. Heatmap of the expression levels of all the genes annotated to the ontologies related to immune response (9 genes) in the lapatinib-treated group *vs.* the control. **B, C** HaCaT cells and NHEK cells were treated with lapatinib and the mRNA expression of *TNFA, IL6, CCL2* and *IL18* were analyzed by RT-qPCR. **D** HaCaT cells were treated with or without 4 μM lapatinib for 48 h, then the supernatant was collected and the secretory levels of TNFA and IL6 were detected by ELISA assay. The *P* value was calculated by Student's *t* test (unpaired, two-tailed, 2 groups) or by one-way ANOVA (Dunnett's multiple comparisons test or Sidak test). *n.s.*, no significance; **P* < 0.05; ***P* < 0.01; ****P* < 0.001; *****P* < 0.0001.

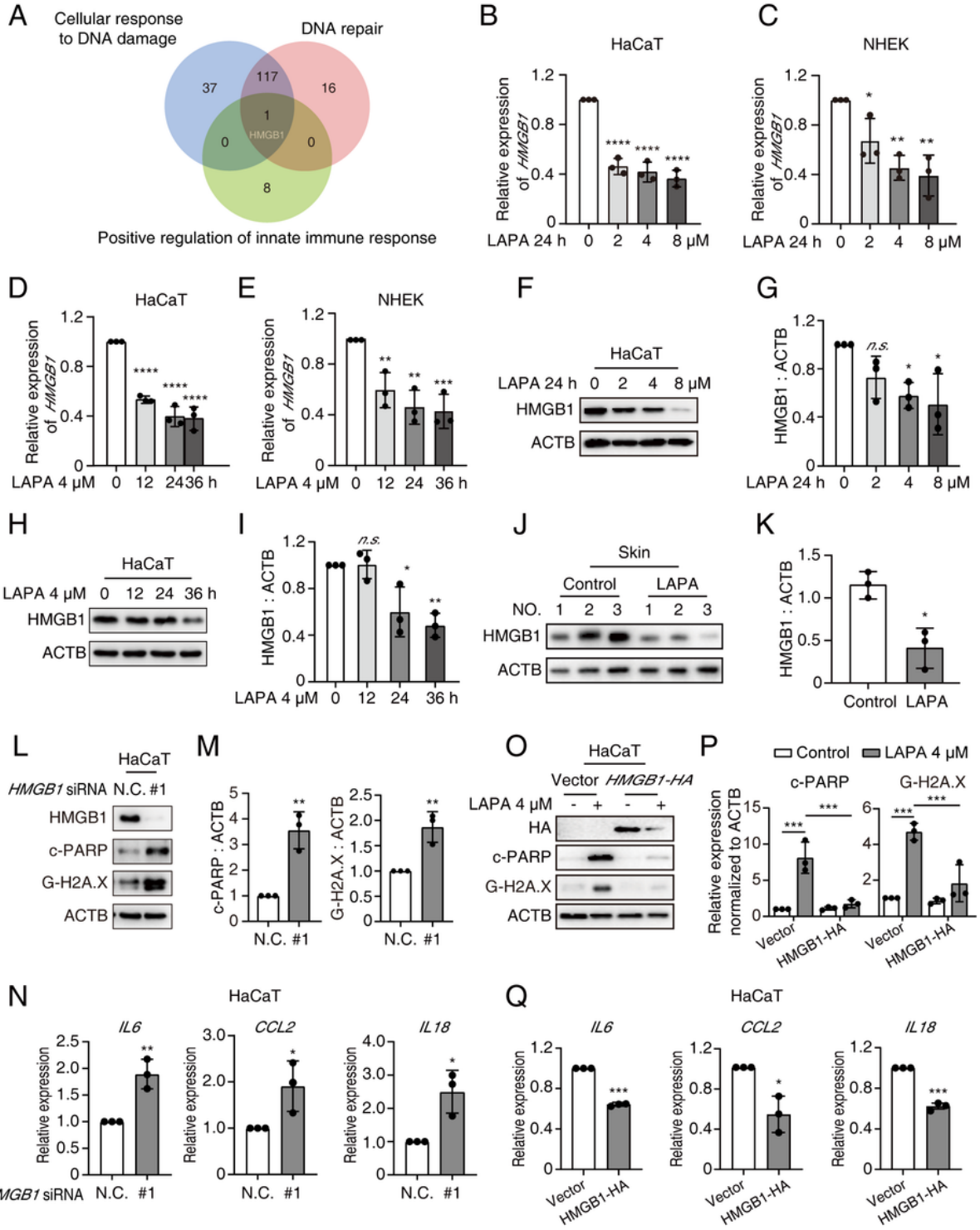

Figure 6

Lapatinib decreases the expression level of HMGB1 by transcriptional inhibition.

A HaCaT cells were treated with or without 4 μM lapatinib and performed with RNA-Seq analysis. Venn diagram presenting the overlap of expressed genes along with three biological processes. **B, C** HaCaT cells and NHEK cells were treated with 0, 2, 4 and 8 μM lapatinib for 24 h and the mRNA level of *HMGB1*

was detected by RT-qPCR. **D, E** HaCaT cells and NHEK cells were treated with 4 μM lapatinib for 0, 12, 24 or 36 h, and the mRNA level of HMGB1 was detected by RT-qPCR. **F, G** Representative immunoblots of HMGB1 proteins in HaCaT cells stimulated with lapatinib. **H, I** HaCaT cells were treated with 4 μM lapatinib for the indicated times, and the protein level of HMGB1 was analyzed by western blot. **J, K** Total mouse skin tissue lysates were analyzed by western blots using an anti-HMGB1 antibody. Densitometric analysis was carried out. **L-N** HaCaT cells were transfected with nontargeting siRNA (N.C.) or siRNA targeting *HMGB1*. **L, M** The protein levels of c-PARP and G-H2A.X were detected by western blot. **N** RT-qPCR was performed to detect the mRNA levels of *IL6, CCL2* and *IL18*. **O-Q** HaCaT cells were transfected with *pcDNA3.0-HMGB1* plasmid or vector and exposed to 4 μM lapatinib for 24 h. **O, P** The protein levels of c-PARP and G-H2A.X. Western blot was repeated three times and densitometric analysis was carried out. **Q** The mRNA levels of *IL6, CCL2* and *IL18* were analyzed. The *P* value was calculated by Student's *t* test (unpaired, two-tailed, 2 groups) or by one-way ANOVA (Dunnett's multiple comparisons test or Sidak test). *n.s.*, no significance; **P* < 0.05; ***P* < 0.01; ****P* < 0.001; *****P* < 0.0001.

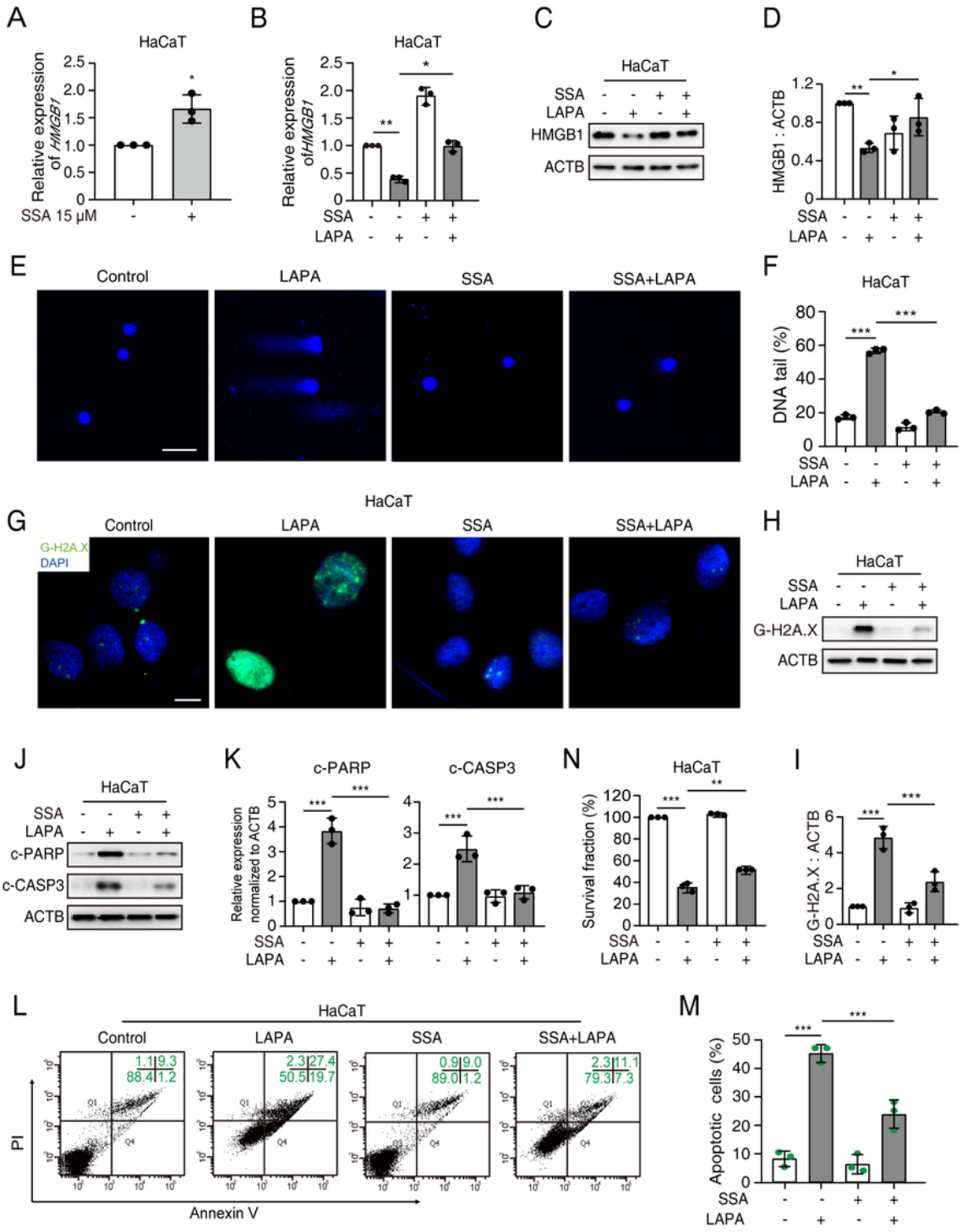

Figure 7

Saikosaponin A alleviates lapatinib-induced DNA damage and apoptosis by inhibiting lapatinib-induced downregulation of HMGB1. HaCaT cells were exposed to saikosaponin A (15 μM) or/and lapatinib (4 μM) for 24 h. **A, B** The mRNA level of *HMGB1* was detected by RT-qPCR. **C, D** The protein level of HMGB1 was analyzed by western blot. **E** HaCaT cells were treated with 15 μM saikosaponin A or/and 4 μM lapatinib for 24 h, immunofluorescence assay was performed to detect the expression of G-H2A.X. Scale bars: 10

μm. **F, G** Represent images of DNA damage detected by comet assay. Scale bars: 100 μm. Quantitative analysis was performed on the percentage of DNA tail. **H, I** Expression of G-H2A.X was analyzed by western blot. **J, K** The protein levels of c-PARP and c-CASP3 were analyzed by western blot and corresponding densitometric analysis was performed. **L, M** The apoptosis rates were analyzed by flow cytometry with PI/Annexin V double staining. Three independent experiments were performed and the data were shown as Mean ± SD. **N** SRB assay was used to assess the effect of saikosaponin A on the survival fraction reduced by lapatinib. Three independent experiments were performed and the data were shown as Mean ± SD. The *P* value was calculated by one-way ANOVA (Dunnett's multiple comparisons test or Sidak test). **P* < 0.05; ***P* < 0.01; ****P* < 0.001.

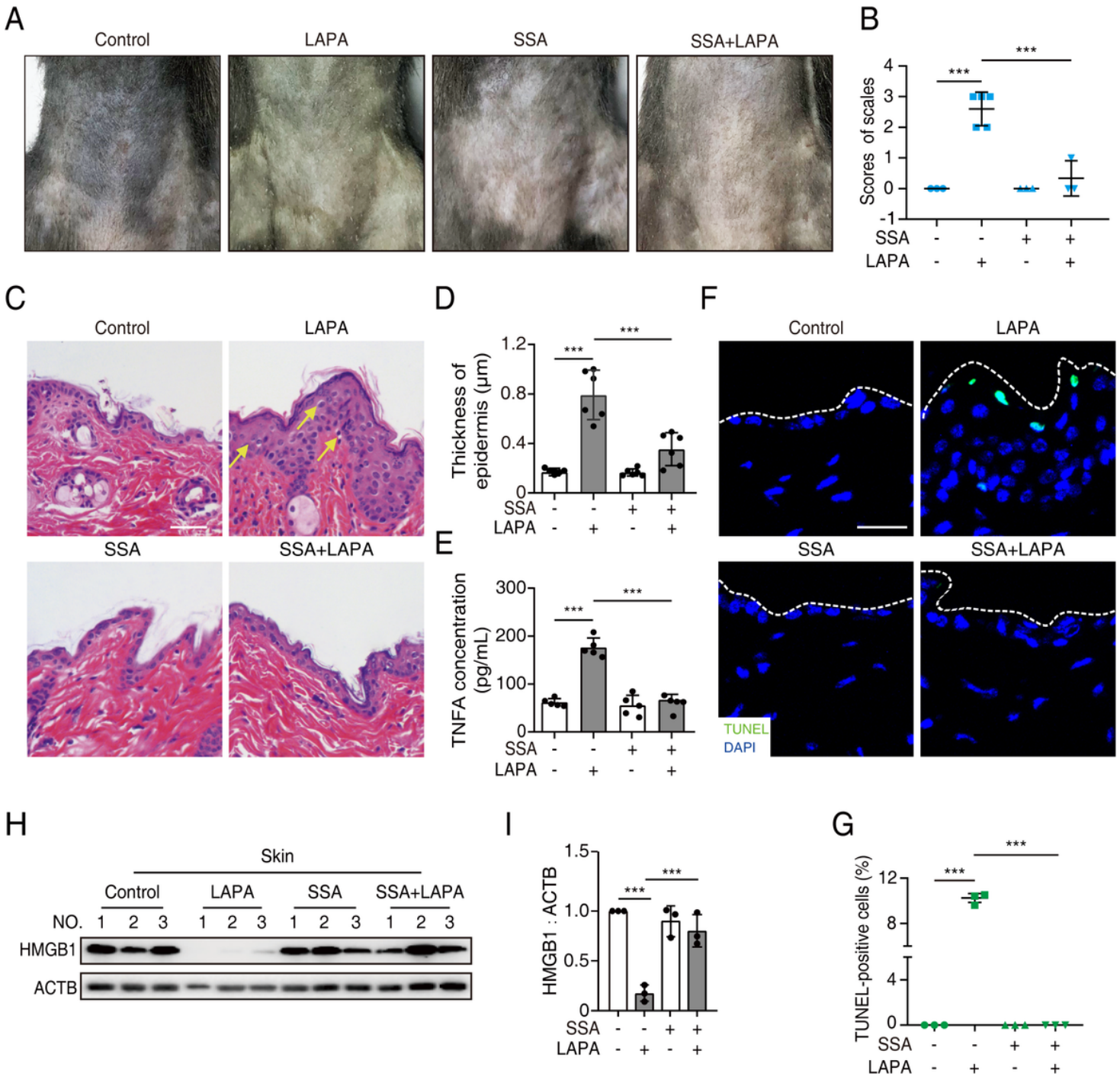

Figure 8

Saikosaponin A alleviates lapatinib-induced cutaneous toxicity by inhibiting lapatinib-induced downregulation of HMGB1. **A-G** C57BL/6 mice were administered with 0.5% CMC-Na, lapatinib (950 mg/kg) or/and saikosaponin A (20 mg/kg) for 28 days, and skin tissues were harvested after mice were sacrificed. **A** Representative images of scales from the control, lapatinib, saikosaponin A or combination group. **B** The score of scales according to the clinical manifestation criteria were shown. **C, D** Microscope images of H&E staining performed on the epidermal layer of mice. Scale bars: 25 μm. Quantitative

analysis of the epidermal layer thickness was shown. **E** ELISA assay showing the effect of saikosaponin A on the secretion of TNFA. **F, G** Representative images of skin tissues with TUNEL staining (green) and nuclear counterstaining (blue) of skin tissue. TUNEL-positive cells were analyzed. Scale bars: 100 μm. **H, I** C57BL/6 mice were administered with 0.5% CMC-Na, lapatinib (950 mg/kg) or/and saikosaponin A (20 mg/kg) for 28 days. Skin tissues were harvested after the mice were sacrificed and total tissue lysates were prepared. The protein level of HMGB1 was analyzed by western blot and ACTB was used as a loading control. The *P* value was calculated by one-way ANOVA (Sidak test). ***$P < 0.001$.

Supplementary Files

This is a list of supplementary files associated with this preprint. Click to download.

- Supplementalfigure11.tif
- Supplementalfigure21.tif
- Supplementalfigure31.tif
- SupplementalFigure41.tif
- SupplementalFigure51.tif
- SupplementalFigure61.tif